eNeuro

Research Article: New Research | Sensory and Motor Systems

Neural evidences of hierarchical cognitive control during haptic processing: an fMRI study

Ane Gurtubay-Antolin[1,2], Patricia León-Cabrera[1,2] and Antoni Rodríguez-Fornells[1,2,3]

[1]*Cognition and Brain Plasticity Group [Bellvitge Biomedical Research Institute- IDIBELL], 08097, L'Hospitalet de Llobregat, Barcelona, Spain*

[2]*Dept. of Cognition, Development and Education Psychology, Campus Bellvitge, University of Barcelona, L'Hospitalet de Llobregat, 08907, Barcelona, Spain*

[3]*Catalan Institution for Research and Advanced Studies (ICREA), 08010, Barcelona, Spain*

https://doi.org/10.1523/ENEURO.0295-18.2018

Received: 19 July 2018

Revised: 29 August 2018

Accepted: 2 October 2018

Published: 15 November 2018

Author contributions: AGA and ARF Designed research; AGA and PLC Performed research; AGA Analyzed data; AGA, PLC and ARF Wrote the paper.

Funding: Spanish government
PSI2015-69178-P

Conflict of Interest: Authors report no conflict of interest

Funding sources: This study has been funded by Ministerio de Ciencia, Innovación y Universidades, which is part of Agencia Estatal de Investigación (AEI), through the project PSI2015-69178-P (Co-funded by European Regional Development Fund. ERDF, a way to build Europe).

Correspondence should be addressed to Ane Gurtubay Antolin, anegurtubay@gmail.com

Cite as: eNeuro 2018; 10.1523/ENEURO.0295-18.2018

Manuscript title: Neural evidences of hierarchical cognitive control during haptic processing: an fMRI study

Abbreviated title: Supramarginal gyrus and S1 in tactile mismatch

Authors: Ane Gurtubay-Antolin[1,2], Patricia León-Cabrera[1,2] & Antoni Rodríguez-Fornells[1,2,3]†

[1]Cognition and Brain Plasticity Group [Bellvitge Biomedical Research Institute- IDIBELL], 08097, L'Hospitalet de Llobregat, Barcelona, Spain

[2]Dept. of Cognition, Development and Education Psychology , Campus Bellvitge, University of Barcelona, L'Hospitalet de Llobregat, 08907, Barcelona, Spain

[3]Catalan Institution for Research and Advanced Studies (ICREA), 08010, Barcelona, Spain

Author contributions: AGA and ARF Designed research; AGA and PLC Performed research; AGA Analyzed data; AGA, PLC and ARF Wrote the paper.

Correspondence should be addressed to: Ane Gurtubay Antolin
University of Barcelona (Basic Psychology Dept.)
Bellvitge Campus, University of Barcelona
L'Hospitalet de Llobregat, Barcelona, 08097, Spain
Phone: +34 934024268 // Fax: +34 934024268
anegurtubay@gmail.com

Number of figures: 5;

Number of tables: 0

Number of Multimedia: 0

Number of words for Abstract: 249

Number of words for Significance Statement: 103

Number of words for Introduction: 602

Number of words for Discussion: 1469

Acknowledgements: The authors thank David Cucurell for his help.

Conflict of Interest: Authors report no conflict of interest

Funding sources: This study has been funded by Ministerio de Ciencia, Innovación y Universidades, which is part of Agencia Estatal de Investigación (AEI), through the project PSI2015-69178-P (Co-funded by European Regional Development Fund. ERDF, a way to build Europe).

ABSTRACT

Interacting with our immediate surroundings requires constant manipulation of objects. Dexterous manipulation depends on comparison between actual and predicted sensory input, with these predictions calculated by means of lower- and higher-order corollary discharge signals. However, there is still scarce knowledge about the hierarchy in the neural architecture supporting haptic monitoring during manipulation. The present study aimed to assess this issue focusing on the cross-talk between lower-order sensory and higher-order associative regions. We used functional magnetic resonance imaging in humans during a haptic discrimination task in which participants had to judge whether a touched shape or texture corresponded to an expected stimulus whose name was previously presented. Specialized haptic regions identified with an independent localizer task did not differ between expected and unexpected conditions, suggesting their lack of involvement in tactile monitoring. When presented stimuli did not match previous expectations, the left supramarginal gyrus, middle temporal, and medial prefrontal cortices were activated regardless of the nature of the haptic mismatch (shape/texture). The left SI responded differently to unexpected shapes and textures in line with a specialized detection of haptic mismatch. Importantly, connectivity analyses revealed that the left supramarginal gyrus and SI were more functionally coupled during unexpected trials, emphasizing their interaction. The results point for the first time to a hierarchical organization in the neural substrates underlying haptic monitoring during manipulation with the supramarginal gyrus as a higher-order hub comparing actual and predicted somatosensory input, and SI as a lower-order site involved in the detection of more specialized haptic mismatch.

SIGNIFICANCE STATEMENT

The findings in the present study have important implications for the understanding of the neural architecture that supports haptic monitoring during manipulation. The results point, for the first time, to a hierarchical organization in the neural substrates underlying haptic monitoring during manipulation. In this hierarchy, the supramarginal gyrus is positioned as a higher-order region comparing predicted and actual somatosensory input, and SI as a lower-order site involved in the detection of more specialized haptic mismatches. The increased functional connectivity between the supramarginal gyrus and SI during the processing of unexpected stimuli emphasizes the cross-talk between lower-order sensory and higher-order associative regions during manipulation.

INTRODUCTION

Interacting with our immediate surroundings requires constant manipulation of objects. Dexterous manipulation (sequences of somatosensory events linked to subgoals) requires that monitoring mechanisms (controllers) adapt motor commands to the relevant physical properties of the target object (Johansson and Westling, 1988). Motor commands are based on both the previously stored sensorimotor memory representations of objects (Johansson and Cole, 1992) and the current state of the motor apparatus (which depends on previous representations of the body in terms of proprioceptive information) (Giummarra et al., 2008). Furthermore, information about the surface properties of the object is provided by somatosensory afferents in the hand. In particular, this relies mainly on the timing and firing-rate of slow- and fast-adapting afferent populations (FA-I and SA-I) that can discriminate different surface curvatures after as few as five afferents have begun firing (Johansson and Westling, 1987; Johansson and Birznieks, 2004).

In order to regulate haptic monitoring, controllers compare the actual sensory input with the expected sensory consequences of initiated motor commands by means of the *efference copy* (Feinberg, 1978; Frith, 2014; Wolpert and Miall, 1996). This copy of efferent motor commands allows calculating how self-generated movement might influence the input sensory signal as well as maintaining performance in the presence of feedback delays. In other words, these predictions are necessary, taking into account that sensorimotor monitoring loops involved in corrective actions have long time delays (~ 100 ms) (Johansson and Flanagan, 2008). Of note, in addition to the *efference copy* (where a copy of the motor commands issued to an effector is projected to low-level somatosensory neurons) (Von Holst and Mittelstaedt, 1950), the information transfer from motor to sensory areas might also occur at multiple levels, leading to the distinction of lower- and higher-order (corollary discharge) CD signals (Crapse and Sommer, 2008). Lower-order CD signals regulate the sensory information that enters the system whereas higher-order CD signals implement adjustments in anticipation of the sensory input, facilitating the contextual interpretation of sensory information. In order to combine these two types of signals, the interplay between lower-order sensory areas and higher-order associative regions is crucial. Despite previous literature supporting the hierarchical nature of haptic processing (Bodegard et al., 2001; Bohlhalter et al., 2002; Kassuba et al., 2013; Sathian et al., 2011), there is still scarce knowledge regarding the hierarchy of the neural substrates underlying haptic monitoring and how these two types of information are implemented by local and global networks.

The present study assessed this issue by focusing on the cross-talk between lower-order somatosensory and higher-order associative regions. To address this, we first identified, using an independent localizer task, lower-order somatosensory regions that process shapes or textures selectively. Afterwards, we conducted a haptic discrimination task in which

unexpected shapes and textures were presented in order to trigger monitoring mechanisms involved in the comparison between predicted and actual sensory input. We assessed whether the specialized haptic areas identified with the localizer task distinguished expected from unexpected (50%) stimuli in the category they were suited to process. We also conducted a whole brain analysis to identify higher-order areas involved in haptic monitoring. We hypothesized that higher-order associative regions supporting haptic monitoring during manipulation would respond similarly regardless of the nature of the haptic mismatch, independently of whether it was a shape or texture mismatch. Some of these areas (the highest in the hierarchy) might even serve to detect mismatches in other sensory modalities. In contrast, we expected to see different patterns of response in specialized somatosensory regions (e.g. somatosensory cortices or areas selectively responding to haptic exploration of shapes and textures) depending on the type of tactile property (shape or texture) violating the expectation.

MATERIALS AND METHODS

2.1 Participants. Twenty-two right-handed participants (13 female, mean age = 23.2 ± 1.4 years) took part in the experiment. For the localizer task, the data of twenty subjects were analyzed, since two subjects were excluded from the fMRI analysis. One subject was excluded due to anomalous cortical response to tactile events; they did not elicit activity in the somatosensory cortex. Moreover, the logfile of another participant was not generated. For the haptic discrimination task, three additional subjects were excluded from the fMRI analysis since their responses were not recorded. Hence, the fMRI analysis of the haptic discrimination task included seventeen participants (12 female, mean age = 23.4 ± 1.5 years). The experiment was undertaken with the understanding and written consent of each participant and was approved by the local ethics committee in accordance with the Declaration of Helsinki.

2.2 Procedure and general experimental design. Before the single scanning session participants underwent a training phase that lasted about 30 min. During the training phase, they became familiarized with the haptic stimuli (used in both the independent localizer task and the haptic discrimination task) and the experimental procedure. Since inside the scanner all the instructions were vocally presented, the meaning of each auditory cue was explained and a brief simulation was conducted. Participants lay supine in the scanner and were blindfolded during the entire scanning session. First, the T1 structural image was acquired. To avoid circularity (Kriegeskorte et al., 2008), an independent functional localizer task was then conducted to localize areas typically involved in haptic processing shape and texture (from here on referred to as 'Property-selective Haptic ROIs') (Amedi et al., 2001). Lastly, the haptic discrimination task was conducted, to assess whether the previously identified haptic-specialized areas distinguished expected from unexpected stimuli and to establish higher-order regions involved in the detection of haptic incongruencies. Note that these higher-order areas are not selective to haptic processing and thus could not be spotted by the independent localizer task.

2.2.1 Independent functional localizer task

Stimuli. For the localizer task, we used six real 3D objects (pen cap, thread spool, eye drop bottle, clothespin, bottle cork, and mini pencil) and six textures, approximately 4 x 4 cm (corduroy, cork, sackcloth, sandpaper, sponge, and scourer), presented in a rotating tray (see panel A in **Figure 1**).

Design. Participants were asked to palpate sequences of shapes or textures presented in a rotating tray and covertly recognize them. The task began with a 10 sec resting interval that was not analyzed. We used a block design that consisted of a single run with two haptic conditions (Shape, Sh; Texture, Tx) and a Rest condition (see panel B in **Figure 1**). All

blocks lasted 15 sec and Sh and Tx blocks were alternated between each pair of Rest blocks. Each haptic block consisted in palpating (4 sec/palpation) three stimuli placed in a quarter of the rotating tray and then spinning the tray to continue with the next quarter (after the resting period) (see panel C in **Figure 1**). The hand always palpated the sequence of objects in the same order since the location of the stimuli was previously known. The task lasted approximately 5 min.

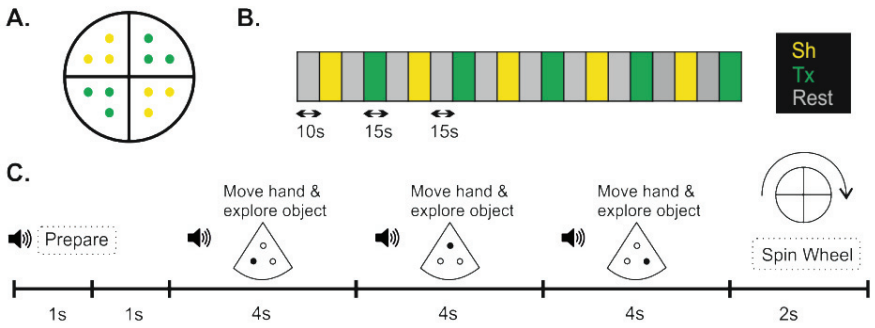

Figure 1. Stimuli and procedure used in the localizer task. A. Stimuli: Rotating tray with three objects (shapes: yellow) or three textures (green) in each quarter. Shapes were real 3D objects: pen cap, thread spool, eye drop bottle, clothespin, bottle cork, and mini pencil. Textures, approximately 4x4 cm, were corduroy, cork, sackcloth, sandpaper, sponge, and scourer. B. Block design for the single run. The run comprised 10 haptic blocks (yellow-shape; green-texture) and began with a 10 sec interval that was not analyzed. The order of the haptic blocks was alternated. C. Procedure for a haptic block. The block began with an auditory cue indicating that the haptic block would begin. After 1 sec of silence, the first auditory cue indicated to the participant the first (of the sequence of three) stimulus and to palpate it. After 4 sec of exploration, a second (and third) auditory cue indicated to move the hand towards and palpate the second (and third) stimulus. The hand always moved in the same direction when ranging from one stimulus towards the next one since the location of the stimuli was previously known. To conclude, an auditory cue instructed the participants to spin the tray (in order to prepare it for the next block) and rest.

2.2.2 Haptic discrimination task

Stimuli. 25 three-dimensional haptic stimuli were manufactured, measuring approximately 4 x 4 x 2 cm and varying in shape and texture. The 25 stimuli comprised a variety of 5 shapes (flower, circle, heart, square, and star) that were covered with 5 textures (corduroy, sandpaper, plastic, paper, and expanded polystyrene) (see panel A in **Figure 1**). Thus, each stimulus had 2 properties: a particular shape and a particular texture (e.g., circle of corduroy, circle of paper etc.). All the stimuli were chosen so as to be easily identifiable and the 5 shapes were previously used in two other studies (see Gurtubay-Antolin et al., 2015; Gurtubay-Antolin et al., 2016, submitted).

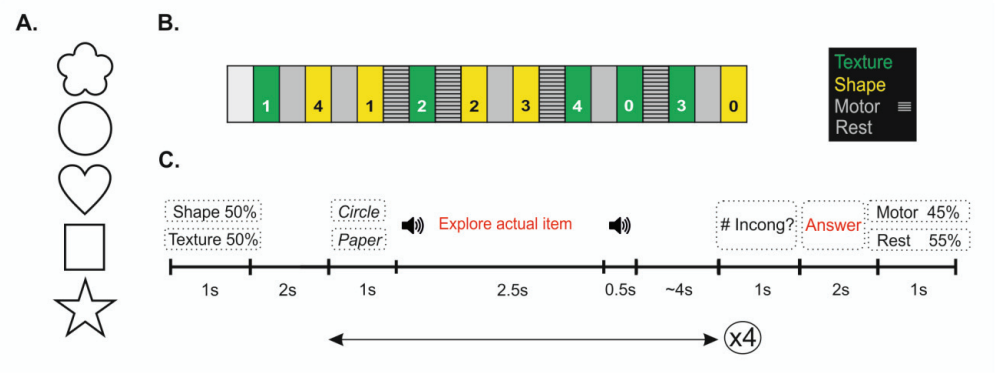

Figure 2. Stimuli and procedure used in the haptic discrimination task. A. Stimuli: Variety of 5 shapes (flower, circle, heart, square, and star). The 25 haptic stimuli were manufactured covering each of the 5 shapes with 5 textures (corduroy, sandpaper, plastic, paper, and expanded polystyrene). B. Block design for one run. Each run comprised 10 haptic blocks (green-attend texture; yellow-attend shape) and began with a 10 sec interval that was not analyzed. The order of the haptic blocks was randomized. Between two haptic blocks, Rest or Motor blocks were presented in randomized order. In each haptic block, 4 haptic trials where presented (see Panel C for further information on haptic blocks). The number in each block corresponds to the number of incongruent trials presented in that block (ranging from a minimum of 0 to a maximum of 4). For a particular dimension (shape/texture), the number of incongruent trials within each block was not repeated in that run. C. Procedure for a haptic block. The block began with an auditory cue instructing as to the dimension of the object that had to be attended to (50% shape, 50% texture). After a 2 sec interval, the first haptic trial started. In each haptic trial the name of an expected item was presented and an auditory cue indicated that the exploration of the actual item could begin. In half of the trials the word delivered by the headphones corresponded to the touched object (congruent), and in the other 50% of trials the object did not match the

name (incongruent). We therefore had 6 conditions (4 corresponding to all the possible combinations--congruent shape (CSh), incongruent shape (ISh), congruent texture (CTx), and incongruent texture (ITx)--and two additional control conditions, Motor (M) and Rest (R)). Free exploration was allowed. 2.5 sec later, a second auditory cue indicated that the exploration period was over. After a jittering period, the next haptic trial could start. After 4 haptic trials, the participants were asked about the number of incongruent trials. Using their left hand, participants had to push a button as many times as the incongruent trials that had been presented (ranging from 0 to 4). To conclude, an auditory cue indicated whether a 'Rest' or 'Motor' block followed (a block in which participants were asked to move the fingers as they were exploring an imaginary object).

Design. Participants were presented with brief sequences of objects or textures to palpate and had to judge whether a touched stimulus corresponded to an expected stimulus whose name had been previously presented orally. Subjects were placed with the right hand facing upward and the stimuli were placed into the subject's palm by the experimenter. The experiment was designed as a mixed block/event-related design with two haptic conditions (Shape, Sh; Texture, Tx) in which subjects were instructed to attend to the shape or the texture of the stimuli (block design), a control motor condition (Motor) in which they were asked to move their fingers as they were exploring an imaginary object (and were explicitly instructed not to touch themselves), and a 'Rest' condition.

The experimental design consisted of 4 runs and each run comprised 10 haptic blocks (5 Sh, 5 Tx), 4 Motor blocks, and 5 Rest blocks (see panel B in **Figure 2**). All the runs began with a 10 sec resting interval that was not analyzed. The type of haptic block (shape or texture) was randomized and lasted 32 sec. Each haptic block consisted of 4 consecutive somatosensory trials (8 sec each if we take into account the ~ 4 s jittering interval). Each haptic block began with an auditory cue indicating the dimension of the object that had to be attended (50% shape, 50% texture). After a 2 sec interval, the first haptic trial started (see panel C in **Figure 2**). In each haptic trial the name of an expected stimulus was vocally presented and a second later, an auditory cue indicated that the exploration of the actual

stimulus could begin. In half of the trials the word delivered by the headphones corresponded to the touched object (congruent, C), and in the other 50% of trials the object did not match the name (incongruent, I). All the possible combinations were presented the same number of times. We therefore had 6 conditions (4 corresponding to all the possible combination--congruent shape (CSh), incongruent shape (ISh), congruent texture (CTx) and incongruent texture (ITx)--and two additional control conditions, motor (M) and rest (R)). Free exploration was allowed. 2.5 sec later, a second auditory cue indicated that the exploration period was over. After a jittering period ranging from 2 to 6 sec in 100 ms intervals (mean = 4 sec), the next haptic trial could start. After 4 haptic trials, the subjects were asked about the number of incongruencies detected in the preceding block. Using their left hand, participants had to push a button as many times as there were identified incongruent trials (ranging from 0 to 4). For a particular dimension (Sh or Tx), the number of incongruent trials within each block was not repeated in that run. Between two haptic blocks, 10 sec Rest or Motor blocks were presented in randomized order.

2.3 Behavioral analysis. We considered a correct response block each time the number of incongruencies presented in a haptic block and the number of times the participant had pushed the button matched. The percentage of correct responses served (i) to rule out blocks with erroneous responses from the fMRI analysis, and (ii) to obtain an overall estimate of the performance.

2.4 Image acquisition. Scanning was performed on a 3-T Siemens Trio System. Functional data were acquired using a gradient echo pulse sequence (32 transverse slices oriented along the anterior-posterior commissural axis with a 30-degree upward tilt to avoid the eyes, repetition time of 2 sec, echo time of 30 ms, 3 x 3 x 3.5 mm voxels, 0.8-mm interslice gap). A high-resolution T1-weighted magnetization-prepared rapid acquisition gradient echo

(MPRAGE) image (240 slices sagittal, TR = 2300 ms, TE = 2.98 ms, 1 mm isotropic voxels) was also collected.

2.5 Image processing and statistical analysis. fMRI data were analyzed using standard procedures implemented in the Statistical Parametric Mapping software (SPM8, Wellcome Trust Centre for Neuroimaging, University College, London, UK, www.fil.ion.ucl.ac.uk/spm/). The preprocessing consisted of several steps: realignment, segmentation, normalization, and smoothing. To correct head-movement artefacts based on an affine rigid body transformation, images were spatially realigned with respect to the first volume of the first run (Friston et al., 1996). Each participant's MPRAGE scan was co-registered to the mean echo planar imaging (EPI) volume, produced in the previous step during spatial realignment. Each coregistered structural scan was then segmented using New Segment (Ashburner and Friston, 2005). Then the flow fields containing the deformation parameters of this template were used to normalize each participant's realigned EPIs to MNI space. Finally, normalized EPI images were re-sliced to 2 x 2 x 2 mm and smoothed with an 8 mm FWHM Gaussian kernel (Ripolles et al., 2016;Ripolles et al., 2014).

2.5.1 Independent functional localizer task

We aimed to identify specialized haptic regions responding differentially to the exploration of shapes and textures (Property-selective Haptic ROIs) in order to analyze their involvement in tactile monitoring. To avoid circularity (Kriegeskorte et al., 2008) the ROIs were created using independent data obtained from the independent localizer task. For the independent functional localizer task, a block design matrix was specified using the canonical hemodynamic response function. Block onsets were modeled at the moment at which participants heard the auditory cue that indicated that they could start palpating the first of the three stimuli placed in a quarter of the rotating tray. First-level statistical analysis

was based on a least square estimation using the general linear model. Individual brain responses to the 'Shape' and 'Texture' conditions were modeled with a regressor waveform convolved with a canonical hemodynamic response function. Movement parameters (estimated during the realignment phase) were also included in the model as covariates of no interest to correct for motion effects as well as as constant vectors. Linear contrast images for the main effect of haptic processing (Sh + Tx > Rest) and the main effect of property (Sh > Tx and viceversa) were calculated for each subject, and statistical parametric maps (SPMs) were generated. Group activation was calculated using a random effects model, accounting for inter-subject variance. Main effects of haptic processing were only used for sanity checks to confirm that they activated sensorimotor cortical areas. 'Property-selective Haptic ROIs' were created entering individual contrast images into a second level one sample t-test to test for (i) main effects of shape (Sh > Tx) and (ii) main effects of texture (Tx > Sh) ($p_{uncorrected}$ = 0.005, k=50). In order to maximize sensitivity within our ROIs, we performed a meta-analysis using NeuroSynth (a platform for large-scale, automated meta-analysis of fMRI data; www.neurosynth.org; (Yarkoni et al., 2011) [see (Ripolles et al., 2016) for a similar approach]. We put together a term-based search for 'tactile' that resulted in 190 studies (search performed on October 20, 2016). Then, a forward inference mask (which represented the probability that the term 'tactile' was associated with a particular activation) was generated (corrected at p_{FDR} = 0.01). We then refined the previously created ROIs by masking them with the results of the NeuroSynth meta-analysis. In other words, each final ROI contained only voxels that were part of the original ROIs and that were also tactile-related according to the meta-analysis.

2.5.2 Haptic discrimination task

For the haptic discrimination task, an event-related design matrix was specified using the canonical hemodynamic response function. Trial onsets were modeled at the moment at

299 which participants heard the auditory cue that indicated that they could palpate the stimuli.
300 We only analyzed blocks with correct responses (blocks where the number of presented
301 incongruencies matched the times the participant pushed the response button). Blocks with
302 incorrect responses were not analyzed. First-level statistical analysis was based on a least
303 square estimation using the general linear model. Individual brain responses to the different
304 conditions [congruent shape (CSh), incongruent shape (ISh), congruent texture (CTx),
305 incongruent texture (ITx), and motor (M)] were modeled with a regressor waveform
306 convolved with a canonical hemodynamic response function. Movement parameters
307 (estimated during the realignment phase) were also included in the model as covariates of no
308 interest to correct for motion effects as well as constant vectors.

309 *ROI analysis*

310 First, a region of interest (ROI) analysis was performed using the results from the
311 independent functional localizer task. To assess whether 'Property-selective Haptic ROIs'
312 could detect conflicting haptic information in the category they were suited to process,
313 paired t-tests were conducted. We compared mean beta values (i) between CSh and ISh
314 conditions in ROIs selective to shape processing and (ii) between CTx and ITx in ROIs
315 selective to texture processing. The significance threshold was corrected for multiple
316 comparisons taking into account the number of ROIs.

317 *Whole brain analysis*

318 Additionally, to identify higher-order areas involved in haptic monitoring, a whole brain
319 analysis was conducted. Linear contrast images for (i) the main effect of haptic processing
320 with the related motor component (CSh + ISh + CTx + ITx > R), (ii) motor processing
321 without somatosensory stimulation (M > R), (iii) somatosensory stimulation without motor
322 processing (CSh + ISh + CTx + ITx > M), (iv) the main effect of shape (CSh + ISh > CTx +

ITx), and (v) the main effect of texture (CTx + ITx > CSh + ISh) were calculated to perform some sanity tests. These tests aimed to confirm that the previous contrasts activated (i) sensorimotor cortical areas, (ii) motor, but not somatosensory, areas, (iii) somatosensory, but not motor, areas, and (iv) previously reported areas specifically processing shapes as opposed to textures and (v) vice versa.

To identify regions involved in haptic monitoring, linear contrast images for (i) the main effect of congruency (CSh + CTx > ISh + ITx), (ii) the main effect of incongruency (ISh + ITx > CSh + CTx), and the interaction terms (iii) for greater shape incongruency (ISh - CSh > ITx - CTx) and (iv) for greater texture incongruency (ITx - CTx > ISh - CSh), were calculated for each subject. Statistical parametric maps (SPMs) were generated. Group activation was calculated using a random effects model, accounting for inter-subject variance. To test for the main effect of incongruency (ISh + ITx > CSh + Ctx and the reverse) and the interaction term (ISh - CSh > ITx – CTx and the reverse), the individual contrast images were entered into a second level repeated measures ANOVA with 2 within subjects factors (Property and Congruency) and 2 levels each (Shape, texture--Sh and Tx-- and congruent, incongruent--C and I,--respectively). The results were thresholded at $p = 0.05$ FWE corrected at cluster level, with a cluster-forming (voxel-wise) threshold of $p_{uncorrected} < 0.001$ (Woo et al., 2014;Flandin and Friston, 2017). In cases where clusters were further FWE-corrected at the voxel-level, the voxel-level and the FWE-corrected p-value are explicitly mentioned.

Functional connectivity (PPI)

Psychophysiological interaction (PPI) analyses (Friston et al., 1997;Gitelman et al., 2003) identify voxels in which activity is more closely related to activity in a seed region of interest (seed ROI) in a given psychological context. In the present study, PPI analyses were

347 performed in order to identify brain regions that were more functionally coupled (i) with
348 regions that showed the main effects of incongruency (from now on referred to as 'iROIs')
349 while processing incongruent vs. congruent trials, (ii) main effects of congruency ('cROIs')
350 while processing congruent vs. incongruent trials, and (iii) an interaction between
351 incongruency and property ('IntROIs') while processing shape incongruencies in the
352 opposite direction of texture incongruencies (ISh – CSh > Itx - CTx).

353 Four mm radius spheres were created around the group peaks obtained for (i) iROIs, (ii)
354 cROIs, and (iii) IntROIs. For all participants, individual deconvolved time-series were
355 extracted from all voxels within the seed ROIs. New linear models were generated at the
356 individual level, using three regressors. The first regressor was the activity extracted in the
357 seed area. The second regressor represented the condition as a vector that coded (i) the main
358 effect of incongruency (CSh: -1, ISh: 1, CTx: -1, ITx: 1) for iROIs, (ii) the main effect of
359 congruency (CSh: 1, ISh: -1, CTx: 1, ITx: -1) for cROIs, and (iii) the incongruency x
360 property interaction (CSh: -1, ISh: 1, CTx: 1, ITx: -1) for IntROIs. The third regressor
361 represented the interaction of interest between the first (physiological) and the second
362 (psychological) regressors. This was calculated as the element by element product of the
363 extracted time-series (the first eigenvariate from each voxel in the sphere) and the second
364 regressor. The result of this product was then reconvolved with the canonical hemodynamic
365 response function to create the final PPI regressor (Gitelman et al., 2003). The design matrix
366 also included movement parameters as a regressor of no interest. A significant PPI indicated
367 a change in the regression coefficients between any reported brain area and the seed area,
368 related to the experimental condition (ISh + ITx > CSh + Ctx for iROIs; CSh + CTx > ISh +
369 Itx for cROIs and ISh – CSh > Itx – CTx for IntROIs). The voxels identified in this analysis
370 show a pattern of activity correlated with the seed region. Individual summary statistic
371 images obtained at the first level (fixed effects) analysis were entered in a second-level

(random effects) analysis using a one-sample t-test. The results were thresholded at p = 0.05 FWE corrected at cluster level, with a cluster-forming (voxel-wise) threshold of $p_{uncorrected} < 0.001$ (Woo et al., 2014;Flandin and Friston, 2017).

RESULTS

3.1 Behavioral results

Overall percentage of correct response was 91% (SD = 5) (considering both types of haptic blocks). The accuracies considering each property separately were 92 ± 5 % for shape blocks and 90 ± 9 % for texture blocks, with no significant difference between the two ($t(16) = 0.1$; $p = 0.3$).

3.2 fMRI results

3.2.1 Property-selective Haptic ROI creation from localizer task:

The results revealed a main effect of shape (Sh vs.Tx) in three clusters located in the left anterior intraparietal sulcus (aIPS) [-34 -40 46, $t(19) = 5.49$, k = 53044], in the left lateral occipital complex (LOC) [-48 -66 -6, $t(19) = 3.65$, k = 6044], and in the right LOC [52 -56 -6, $t(19) = 3.10$, k = 3324]. Additionally, a cluster located in the left secondary somatosensory area (SII) - parietal operculum- [-42 -18 24, $t(19) = 5.01$, k = 197] showed a main effect of texture (Tx vs. Sh) (see **Figure 3**).

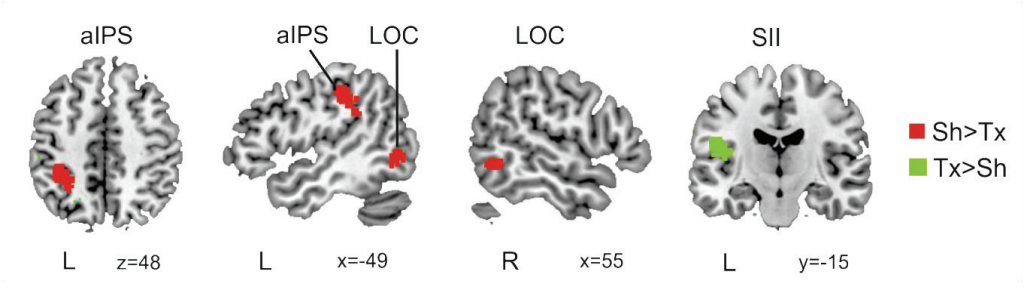

Figure 3. Property-selective Haptic ROI creation from localizer task. In red, regions more active during the haptic shape than texture processing (left aIPS and bilateral LOC). In green, regions more active during the haptic texture than shape processing (left SII--parietal operculum).

3.2.2 Haptic discrimination task:

The average number of trials included in the fMRI analysis was 36 ± 1 (mean ± SD, CSh 37 ± 2; ISh 36 ± 3; CTx 35 ± 5; ITx 35 ± 3). The haptic discrimination task activated a network associated with haptic stimulation, comprising bilateral sensorimotor areas, insulae, posterior parietal cortices, lateral occipital complexes, premotor and supplementary motor areas, prefrontal regions, and thalamus.

Incongruence in property-selective Haptic ROIs

Results of paired t-tests between the CSh and ISh conditions for the three ROIs showing a main effect of shape (Sh vs.Tx) were not significant [left aIPS ($p = 0.2$), left LOC ($p = 0.2$), right LOC ($p = 0.3$), with the significance threshold $p_{BONFERRONI} = 0.05/3 = 0.017$]. Results of a paired t-test between the CTx and ITx conditions for the ROI showing a main effect of texture (Tx vs. Sh) [left SII, parietal operculum ($p = 0.06$)] were not significant, either.

Whole brain analysis: Flexible factorial results

Flexible factorial results revealed important effects of incongruency in a cluster located in the left supramarginal (SMG) (and part of angular) gyrus (iROI1) [-54 -52 24, $t(48) = 5.44$, $p_{FWE\ cluster} < 0.001$, $p_{FWE\ voxel} = 0.03$, $k = 984$], in the left middle temporal gyrus (MTG) (iROI2) [-48 -18 -10, $t(48) = 5.31$, $p_{FWE\ cluster} < 0.001$, $p_{FWE\ voxel} = 0.04$, $k = 744$], and in the medial frontal cortex (mPFC) (iROI3) [-10 54 34, $t(48) = 4.64$, $p_{FWE\ cluster} = 0.003$, $k = 421$] (see **panel A** in **Figure 4**). An important effect of congruency was found in the right primary

414 somatosensory area (SI) (cROI) [58 -16 32, $t(48) = 4.42$, $p_{FWE\ cluster} = 0.04$, k = 235] (see
415 **panel B** in **Figure 4**) as well as a significant interaction of incongruency x property (ISh +
416 ITx > CSh + Ctx) in the left SI (IntROI) [-32 -36 64, $t(48) = 4.39$, $p_{FWE\ cluster} = 0.03$, k = 238]
417 (see **panel C** in **Figure 4**).

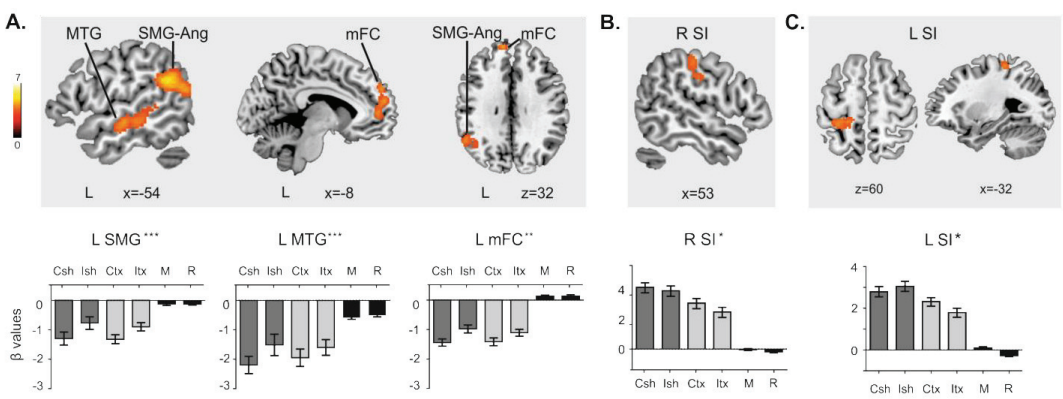

418

419 **Figure 4.** A. Regions active during haptic incongruency revealed by contrasting Incongruent (ISh+ITx) vs.
420 Congruent (CSh+CTx) trials. B. Region active during haptic congruency revealed by contrasting Congruent
421 (CSh+CTx) vs. Incongruent (ISh+ITx) trials. C. Region showing a different pattern of response to shape and
422 texture incongruencies revealed by contrasting Shape Incongruency (ISh-CSh) vs. Texture Incongruency (ITx-
423 CTx) trials. Bar graphs on the lower row show mean beta coefficients within ROIs for each condition of
424 interest (CSh congruent shape, ISh incongruent shape, CTx congruent texture, ITx incongruent texture, M
425 motor--movement without haptic input--, R rest). Ang: Angular gyrus, mFC: medial frontal cortex, MTG:
426 middle temporal gyrus, SI: primary somatosensory cortex, SMG: supramarginal gyrus. R = right hemisphere, L
427 = left hemisphere. MNI coordinates. Maps are thresholded at p FWE cluster-level = 0.001***, p = 0.005**, p =
428 0.05*, (with cluster-forming voxel-wise thresholds of p uncorrected < 0.001) and a minimum cluster size of 50
429 voxels. Note that the clusters in the SMG and MTG are further FWE-corrected at p < 0.05 at the voxel-level.

430

431 *Functional connectivity results*

432 We ran psychophysiological interaction (PPI) analyses in order to further investigate which
433 brain regions showed a significant change in the regression coefficients between that area
434 and the seed area, related to the experimental condition (ISh + ITx > CSh + Ctx for iROIs
435 and ISh – CSh > Itx – CTx for Int ROI), indicating that they were more functionally

coupled. The left SMG (iROI1) showed increased incongruency-related connectivity with a cluster that included the left primary motor area (MI), premotor area, SI, SII, and part of the superior parietal lobe (SPL) [-32 -16 42, $t(16) = 6.21$, $p_{FWE\ cluster} < 0.001$, k = 2045], as well as with a cluster including regions of the right SI and SPL [50 -42 66, $t(16) = 4.93$, $p_{FWE\ cluster} < 0.001$, k = 451]. With a more liberal threshold of $p_{FWE\ cluster} = 0.05$, the left SMG also presented increased connectivity during incongruent trials with a region in the right cerebellum [-20 -48 -28, $t(16) = 5.04$, $p_{FWE\ cluster} = 0.01$, k = 201] (see **panel A** in **Figure 5**). Increased incongruency-related connectivity was also found between the left MTG (iROI2) and the left MI and SI [-46 -22 62, $t(16) = 5.22$, $p_{FWE\ cluster} < 0.001$, k = 546] (see **panel B** in **Figure 5**). The cluster at the left medial frontal cortex (iROI3) did not show any increased incongruency-related connectivity. The cluster in the right primary somatosensory area (cROI) did not show any increased congruency-related connectivity. Lastly, the left SI (IntROI) presented increased connectivity for higher shape incongruency than texture incongruency with the left SMG area [-62 -34 30, $t(16) = 5.98$, $p_{FWE\ cluster} = 0.05$, k = 152] (see **panel C** in **Figure 5**).

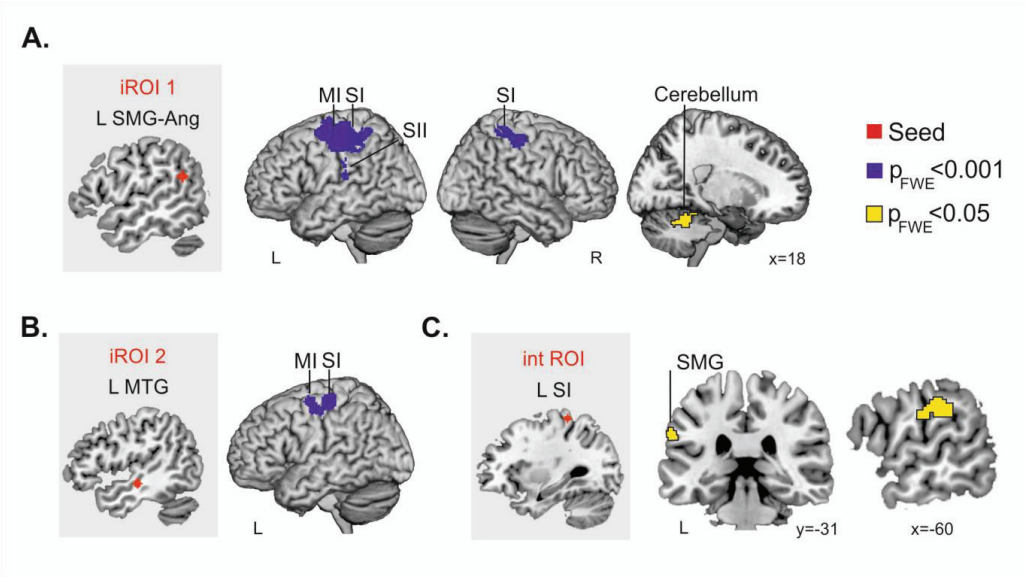

Figure 5. Functional connectivity results (PPI). A. Connectivity results seeding from ROI that showed main effects of incongruency (iROIs) while processing incongruent vs. congruent trials (CSh: -1, ISh: 1, CTx: -1, ITx: 1). Seeds are 4 mm spheres centered at the peak coordinate of the cluster located in left supramarginal-angular gyrus (iROI1) and in left middle temporal gyrus (iROI2) (B). C. Connectivity results seeding from the ROI showing an interaction between incongruency and property (IntROI), while processing shape incongruencies different from texture incongruencies (CSh: -1, ISh: 1, CTx: 1, ITx: -1). Maps are thresholded at p FWE cluster-level = 0.001 and p = 0.05 (with cluster-forming voxel-wise thresholds of p uncorrected < 0.001) and a minimum cluster size of 50 voxels. MI: primary motor cortex, SI: primary somatosensory cortex, SII: secondary somatosensory cortex, SMG: supramarginal gyrus. R = right hemisphere, L = left hemisphere. MNI coordinates.

For further information, unthresholded t-maps resulting from the fMRI analysis have been uploaded to Neurovault (Gorgolewski et al., 2015) [https://neurovault.org/collections/4161/].

DISCUSSION

The present study aimed to elucidate the hierarchy in the neural substrates underlying haptic monitoring during manipulation, focusing on the cross-talk between the lower-order sensory regions and the higher-level associative areas implicated. We found that the anterior intraparietal sulcus, lateral occipital complex, and secondary somatosensory area responded differently to the exploration of shapes and textures, whereas they did not differ between expected and unexpected conditions. This suggests that they are specialized in haptic exploration and processing but are not involved in tactile monitoring. The left supramarginal gyrus, the middle temporal, and the medial prefrontal cortices were activated whenever there was a haptic mismatch, regardless of its nature (shapes and textures alike). In contrast, the activity in the left SI distinguished between unexpected shapes and textures, in line with more specialized haptic mismatch detection. Moreover, the left SMG-Ang area and left SI were more functionally coupled during unexpected trials.

The activity observed in the left SMG-Ang gyrus for unexpected haptic input converges with lesion and functional neuroimaging studies relating this area to comparison processes between predicted and actual sensory consequences of ongoing actions (Sirigu et al., 2004; Desmurget et al., 2009). Prior electrophysiological studies found that the mismatch between internal predictions and reafferent signals elicited a parietally distributed error signal resembling the N400 component (Sirigu et al., 2004; Desmurget et al., 2009), whose main neural substrate has been located in the SMG (Gurtubay-Antolin et al., 2015; Padrao et al., 2016). The functional connectivity analyses revealed that the left SMG-Ang was more functionally coupled during unexpected than expected trials with bilateral sensorimotor regions and the right cerebellum, suggesting a pivotal role of the SMG-Ang area in orchestrating the monitoring of sensory predictions. In this vein, Jelnmalm and colleagues (2006) observed activation in the right SMG area when unexpectedly heavy and light weights were lifted, as well as activity in the left SI and right cerebellum during the lifting of unexpectedly heavy and light weights, respectively. Taken together, these results favor the idea that the controller (SMG-Ang) compares the actual sensory input projected by the early somatosensory cortex with the predictions computed in the cerebellum, made on the basis of proprioceptive information. In fact, the cerebellum is thought to be the keystone computing these predictions since it is widely accepted that it contains internal models of the motor apparatus (Lau et al., 2008; Baumgaertner et al., 2002) and is involved in recruiting internal representations of object properties (Wolpert et al., 1998).

Furthermore, the preponderant left-lateralized (contralateral) activity of the SMG-Ang when manipulating objects with the right hand contrasts with the study by Jenmalm and colleagues (2006), who reported activity in the right SMG even when people used the right hand for lifting. Indeed, a general dominance of the right hemisphere for somatosensory functions has been proposed (Frankenstein et al., 2003). However, aspects such as the selection of the

hand configuration (Naito et al., 2005) might explain the left-lateralized preponderance, which converges with studies reporting greater activation of the left SMG when participants are asked to pantomime object use (Emmorey et al., 2007), or when deaf signers name objects compared to speakers (Rumiati et al., 2004). In this task, the representation of the expected object was available prior to its perception, so participants might have benefited from preparing a hand configuration specific for the expected stimulus.

Different patterns of response were found for unexpected shapes and textures in regions of the left SI, including areas that were functionally connected to the SMG area during incongruence. This supports the notion that a more specialized mismatch detection occurs in the left SI, in line with the view of SI as a lower-order region in the hierarchy of the neural substrates that underlie tactile monitoring. This finding emphasizes the importance of the contralateral SI not only in early somatosensory processing and short-term maintenance of haptic traces (Emmorey et al., 2007), but also in haptic monitoring. In accordance with our results, SI has been seen to participate in decision-making during the haptic choice in a haptic delay task (Kaas et al., 2007; Romo et al., 1999). SI cells showed differential neural activity when monkeys had to choose between different haptic objects, and such differential activity diminished significantly in erroneous trials. In addition, our results show increased functional connectivity between SI and a region in the SMG when unexpected shapes but not textures were presented, pointing to a relevant cross-talk between these regions. However, the right SI did not show increased functional connectivity related to incongruence, highlighting the notion that the functional connections between the left SI and the SMG region are uniquely enhanced by incongruence processing. On the whole, this interplay seems to be important in the detection of haptic expectancy violations, with SI processing more specialized tactile information than the SMG-Ang area.

Lastly, the results suggest that the MTG and the mPFC are additional higher-order regions that work in parallel with the SMG-Ang. During mismatches, the MTG showed increased functional connectivity with the left sensorimotor cortex. The MTG has been observed to respond to deviant stimuli in a tactile oddball task (Wang et al., 2012) and to unexpected touch sensations in monkeys (Allen et al., 2016); thus it seems to be related to violations of predictions selective to the haptic domain. Moreover, the activation found in the mPFC seems to correspond to higher-order cognitive control areas (Perrett et al., 1990). This area has been associated with mismatch detection in several sensory modalities, suggesting its multimodal or amodal nature (Rushworth et al., 2004; Nee et al., 2011). This matches well with our results, which show a lack of functional connections between the mPFC and somatosensory areas (while these are present between the somatosensory regions and the SMG and MTG). There is still debate on this question, as some theories state that the mPFC supports conflict monitoring by calling for control processes to resolve discrepancies (Gaebler et al., 2015; Blakemore et al., 2000; Malekshahi et al., 2016) while a recent line of research suggests that it responds to unexpectedness (Botvinick et al., 2001).

Importantly, the fact that the SMG-Ang, the MTG and the mPFC exhibited negative values in all the haptic conditions might reflect the neuronal inhibition associated with the suppression of items that were not expected (Bursztyn et al., 2006). This inhibition was greater in congruent trials where the actual stimulus matched the expectancy, since the non-expected stimuli had to be inhibited for a longer period. In incongruent trials, the non-expected items were inhibited only until participants realized that the touched stimulus was not the expected one. Subsequently, they might have disinhibited the non-expected items to identify the actual item, even if this was not required in the task. An alternative explanation for these deactivations is that they are associated with the decrease in activity shown by areas of the default mode network (Xu et al., 2016). Recent findings suggest the existence of

552 a gradient in the human cortical organization (which spans from primary sensorymotor
553 cortices to higher order areas whose activity is not specific to a single sensory modality) that
554 is reflected in cortical microstructure and macroscale connectivity (Huntenburg et al., 2018).
555 According to this view, a continuous pattern of connectivity exists between sensorimotor
556 areas that converge in multimodal integration areas, and higher order regions of the default
557 mode network. Our results fit nicely with this interpretation.

558 Of note, the localizer task did not show shape-related activations in sites of the intraparietal
559 sulcus that are typically involved (Sathian, 2016), nor texture-selective activity in the early
560 visual cortex (Sathian et al., 2011; Eck et al., 2013). This raises questions about the actual
561 sensitivity of the localizer task, which may have been affected by the limited amount of time
562 for scanning. Despite this potential limitation, the task revealed 'Property-selective Haptic
563 ROIs' that fit nicely with previous reports of shape-selective activations in the LOC and the
564 IPS (Roland et al., 1998; Sathian et al., 2011), as well as texture-sensitive areas located in
565 the SII--parietal operculum--(Roland et al., 1998). Particularly, the LOC and the IPS are
566 involved not only in haptic perception but also in haptically-guided grasping. This is
567 suggested by the fact that the occipital pole (active during haptic exploration of shapes)
568 shows stronger functional connectivity with the LOC and the IPS during haptic than visual
569 exploration (Monaco 2017) and that the aIPS is sensitive to characteristics of the required
570 grasp (Marangon et al., 2016).

571 Altogether, the results point to a hierarchical organization in the neural substrates underlying
572 haptic monitoring during manipulation, with the supramarginal gyrus as a higher-order
573 region comparing actual and predicted somatosensory input and SI as a lower-order site
574 involved in the detection of more specialized haptic mismatch. We report, for the first time,
575 the functional coupling of these regions during the processing of unexpected tactile stimuli,
576 supporting their pivotal role in haptic monitoring.

577

578 Reference List

579

580 Allen M, Fardo F, Dietz MJ, Hillebrandt H, Friston KJ, Rees G, Roepstorff A (2016)
581 Anterior insula coordinates hierarchical processing of tactile mismatch responses.
582 Neuroimage 127:34-43.

583 Amedi A, Malach R, Hendler T, Peled S, Zohary E (2001) Visuo-haptic object-related
584 activation in the ventral visual pathway. Nat Neurosci 4:324-330.

585 Ashburner J, Friston KJ (2005) Unified segmentation. Neuroimage 26:839-851.

586 Baumgaertner A, Weiller C, Büchel C (2002) Event-related fMRI reveals cortical sites
587 involved in contextual sentence integration. Neuroimage 16:736-745.

588 Blakemore SJ, Smith J, Steel R, Johnstone EC, Frith CD (2000) The perception of self-
589 produced sensory stimuli in patients with auditory hallucinations and passivity experiences:
590 evidence for a breakdown in self-monitoring. Psychological medicine 30:1131-1139.

591 Bodegard A, Geyer S, Grefkes C, Zilles K, Roland PE (2001) Hierarchical processing of
592 tactile shape in the human brain. Neuron 31:317-328.

593 Bohlhalter S, Fretz C, Weder B (2002) Hierarchical versus parallel processing in tactile
594 object recognition: a behavioural-neuroanatomical study of aperceptive tactile agnosia.
595 Brain 125:2537-2548.

596 Botvinick MM, Braver TS, Barch DM, Carter CS, Cohen JD (2001) Conflict monitoring and
597 cognitive control. Psychol Rev 108:624-652.

598 Bursztyn LL, Ganesh G, Imamizu H, Kawato M, Flanagan JR (2006) Neural correlates of
599 internal-model loading. Curr Biol 16:2440-2445.

600 Crapse TB, Sommer MA (2008) Corollary discharge across the animal kingdom. Nat Rev
601 Neurosci 9:587-600.

602 Desmurget M, Reilly KT, Richard N, Szathmari A, Mottolese C, Sirigu A (2009) Movement
603 intention after parietal cortex stimulation in humans. science 324:811-813.

604 Eck J, Kaas AL, Goebel R (2013) Crossmodal interactions of haptic and visual texture
605 information in early sensory cortex. Neuroimage 75:123-135.

606 Emmorey K, Mehta S, Grabowski TJ (2007) The neural correlates of sign versus word
607 production. Neuroimage 36:202-208.

608 Feinberg I (1978) Efference copy and corollary discharge: implications for thinking and its
609 disorders. Schizophr Bull 4:636-640.

610 Flandin G, Friston KJ (2017) Analysis of family-wise error rates in statistical parametric
611 mapping using random field theory. Hum Brain Mapp.

612 Frankenstein U, Wennerberg A, Richter W, Bernstein C, Morden D, Rémy F, Mcintyre M
613 (2003) Activation and deactivation in blood oxygenation level dependent functional
614 magnetic resonance imaging. Concepts in Magnetic Resonance Part A 16:63-70.

615 Friston KJ, Buechel C, Fink GR, Morris J, Rolls E, Dolan RJ (1997) Psychophysiological
616 and modulatory interactions in neuroimaging. Neuroimage 6:218-229.

617 Friston KJ, Williams S, Howard R, Frackowiak RS, Turner R (1996) Movement-related
618 effects in fMRI time-series. Magn Reson Med 35:346-355.

619 Frith CD (2014) The cognitive neuropsychology of schizophrenia. Psychology Press.

620 Gaebler AJ, Mathiak K, Koten JW, Jr., Konig AA, Koush Y, Weyer D, Depner C,
621 Matentzoglu S, Edgar JC, Willmes K, Zvyagintsev M (2015) Auditory mismatch
622 impairments are characterized by core neural dysfunctions in schizophrenia. Brain
623 138:1410-1423.

624 Gitelman DR, Penny WD, Ashburner J, Friston KJ (2003) Modeling regional and
625 psychophysiologic interactions in fMRI: the importance of hemodynamic deconvolution.
626 Neuroimage 19:200-207.

627 Giummarra MJ, Gibson SJ, Georgiou-Karistianis N, Bradshaw JL (2008) Mechanisms
628 underlying embodiment, disembodiment and loss of embodiment. Neuroscience &
629 Biobehavioral Reviews 32:143-160.

630 Gorgolewski KJ, Varoquaux G, Rivera G, Schwartz Y, Ghosh SS, Maumet C, Sochat VV,
631 Nichols TE, Poldrack RA, Poline J-B, Yarkoni T and Margulies DS (2015) NeuroVault.org:
632 a web-based repository for collecting and sharing unthresholded statistical maps of the brain.
633 Front. Neuroinform. 9:8. doi: 10.3389/fninf.2015.00008

634 Gurtubay-Antolin A, Rodriguez-Herreros B, Rodriguez-Fornells A (2015) The speed of
635 object recognition from a haptic glance: event-related potential evidence. J Neurophysiol
636 113:3069-3075.

637 Huntenburg JM, Bazin PL, Margulies DS (2018) Large-Scale Gradients in Human Cortical
638 Organization. Trends Cogn Sci 22:21-31.

639 Johansson RS, Birznieks I (2004) First spikes in ensembles of human tactile afferents code
640 complex spatial fingertip events. Nat Neurosci 7:170-177.

641 Johansson RS, Cole KJ (1992) Sensory-motor coordination during grasping and
642 manipulative actions. Curr Opin Neurobiol 2:815-823.

643 Johansson RS, Flanagan JR (2008) Tactile sensory control of object manipulation in
644 humans. The Senses: A Comprehensive Reference, Academic Press, New York, NY67-86.

645 Johansson RS, Westling G (1987) Signals in tactile afferents from the fingers eliciting
646 adaptive motor responses during precision grip. Exp Brain Res 66:141-154.

647 Johansson RS, Westling G (1988) Coordinated isometric muscle commands adequately and
648 erroneously programmed for the weight during lifting task with precision grip. Exp Brain
649 Res 71:59-71.

650 Kaas AL, Van Mier H, Goebel R (2007) The neural correlates of human working memory
651 for haptically explored object orientations. Cerebral Cortex 17:1637-1649.

652 Kassuba T, Menz MM, Roder B, Siebner HR (2013) Multisensory interactions between
653 auditory and haptic object recognition. Cereb Cortex 23:1097-1107.

654 Kriegeskorte N, Simmons WK, Bellgowan PS, Baker CI (2008) Circular inference in
655 neuroscience: The dangers of double dipping. Journal of Vision 8:88.

656 Lau EF, Phillips C, Poeppel D (2008) A cortical network for semantics:(de) constructing the
657 N400. Nature Reviews Neuroscience 9:920-933.

658 Malekshahi R, Seth A, Papanikolaou A, Mathews Z, Birbaumer N, Verschure PF, Caria A
659 (2016) Differential neural mechanisms for early and late prediction error detection.
660 Scientific reports 6.

661 Marangon M, Kubiak A, Kroliczak G (2016) Haptically Guided Grasping. fMRI Shows
662 Right-Hemisphere Parietal Stimulus Encoding, and Bilateral Dorso-Ventral Parietal
663 Gradients of Object- and Action-Related Processing during Grasp Execution. Front Hum
664 Neurosci 9:691.

665 Naito E, Roland PE, Grefkes C, Choi HJ, Eickhoff S, Geyer S, Zilles K, Ehrsson HH (2005)
666 Dominance of the right hemisphere and role of area 2 in human kinesthesia. Journal of
667 Neurophysiology 93:1020-1034.

668 Nee DE, Kastner S, Brown JW (2011) Functional heterogeneity of conflict, error, task-
669 switching, and unexpectedness effects within medial prefrontal cortex. Neuroimage 54:528-
670 540.

671 Padrao G, Gonzalez-Franco M, Sanchez-Vives MV, Slater M, Rodriguez-Fornells A (2016)
672 Violating body movement semantics: Neural signatures of self-generated and external-
673 generated errors. Neuroimage 124:147-156.

674 Perrett DI, Harris MH, Mistlin AJ, Hietanen JK, Benson PJ, Bevan R, Thomas S, Oram
675 MW, Ortega J, Brierly K (1990) Social Signals Analyzed at the Single Cell Level: Someone
676 is Looking at Me, Something Moved! International Journal of Comparative Psychology 4.

677 Ripolles P, Marco-Pallares J, Alicart H, Tempelmann C, Rodriguez-Fornells A, Noesselt T
678 (2016) Intrinsic monitoring of learning success facilitates memory encoding via the
679 activation of the SN/VTA-Hippocampal loop. Elife 5.

680 Ripolles P, Marco-Pallares J, Hielscher U, Mestres-Misse A, Tempelmann C, Heinze HJ,
681 Rodriguez-Fornells A, Noesselt T (2014) The role of reward in word learning and its
682 implications for language acquisition. Curr Biol 24:2606-2611.

683 Roland PE, O'Sullivan B, Kawashima R (1998) Shape and roughness activate different
684 somatosensory areas in the human brain. Proc Natl Acad Sci U S A 95:3295-3300.

685 Romo R, Brody CD, Hernandez A, Lemus L (1999) Neuronal correlates of parametric
686 working memory in the prefrontal cortex. Nature 399:470-473.

687 Rumiati RI, Weiss PH, Shallice T, Ottoboni G, Noth J, Zilles K, Fink GR (2004) Neural
688 basis of pantomiming the use of visually presented objects. Neuroimage 21:1224-1231.

689 Rushworth MF, Walton ME, Kennerley SW, Bannerman DM (2004) Action sets and
690 decisions in the medial frontal cortex. Trends Cogn Sci 8:410-417.

691 Sathian K (2016) Analysis of haptic information in the cerebral cortex. Journal of
692 Neurophysiology 116:1795-1806.

693 Sathian K, Lacey S, Stilla R, Gibson GO, Deshpande G, Hu X, Laconte S, Glielmi C (2011)
694 Dual pathways for haptic and visual perception of spatial and texture information.
695 Neuroimage 57:462-475.

696 Sirigu A, Daprati E, Ciancia S, Giraux P, Nighoghossian N, Posada A, Haggard P (2004)
697 Altered awareness of voluntary action after damage to the parietal cortex. Nature
698 neuroscience 7:80-84.

699 Von Holst E, Mittelstaedt H (1950) The principle of reafference. Naturwissenschaften
700 37:464-476.

701 Wang L, Li X, Hsiao SS, Bodner M, Lenz F, Zhou YD (2012) Behavioral choice-related
702 neuronal activity in monkey primary somatosensory cortex in a haptic delay task. Journal of
703 cognitive neuroscience 24:1634-1644.

704 Wolpert DM, Miall RC (1996) Forward Models for Physiological Motor Control. Neural
705 Netw 9:1265-1279.

706 Wolpert DM, Miall RC, Kawato M (1998) Internal models in the cerebellum. Trends Cogn
707 Sci 2:338-347.

708 Woo CW, Krishnan A, Wager TD (2014) Cluster-extent based thresholding in fMRI
709 analyses: pitfalls and recommendations. Neuroimage 91:412-419.

710 Xu X, Yuan H, Lei X (2016) Activation and connectivity within the default mode network
711 contribute independently to future-oriented thought. Scientific reports 6:21001.

712 Yarkoni T, Poldrack RA, Nichols TE, Van Essen DC, Wager TD (2011) Large-scale
713 automated synthesis of human functional neuroimaging data. Nat Methods 8:665-670.
714
715